JOURNAL OF PROPULSION AND POWER
Vol. 13, No. 1, January–February 1997

Breakup Processes of Liquid Jets in Subsonic Crossflows

Pei-Kuan Wu,* Kevin A. Kirkendall,† and Raymond P. Fuller‡
Taitech, Inc., Dayton, Ohio 45440
and
Abdollah S. Nejad§
U.S. Air Force Wright Laboratory, Wright–Patterson Air Force Base, Ohio 45433

The breakup processes of liquid jets injected into subsonic air crossflows were experimentally studied. Test liquids, injector diameters, and air Mach numbers were varied to provide a wide range of jet operation conditions. Results indicate that for larger injection velocity conditions liquid jets penetrate relatively far into the crossflows and exhibit surface breakup processes before the column breaks. Liquid column trajectories were correlated by liquid/air momentum flux ratios based on a force analysis of a cylindrical liquid element subjected to an aerodynamic drag force. Drag coefficients were inferred from the column trajectories and were found to exhibit a weak dependence on liquid viscosity. The heights of the column fracture points were correlated using the time required for an analogous droplet to complete an aerodynamic secondary breakup process. The success of the resulting correlation justifies the assumption that the aerodynamic forces acting on a droplet and those acting on a liquid column have similar effects. This result, combined with the trajectory correlation, leads to the conclusion that the liquid column always breaks at the same streamwise location, in agreement with the present experimental observation.

Nomenclature

C_D = drag coefficient, drag/$(0.5\rho_\infty u_\infty^2)$
C_x, C_y = constants for distances to column breakup point
d = injector diameter
M_{air} = Mach number of airstream
Oh_d = Ohnesorge number, $\mu_f/(\rho_f\, d\sigma)^{1/2}$
$\bar{q}$ = liquid/air momentum flux ratio, $\rho_f v_j^2/\rho_\infty u_\infty^2$
Re_{fd} = Reynolds number, $\rho_f\, d v_j/\mu_f$
Re_{gd} = Reynolds number, $\rho_\infty\, d u_\infty/\mu_\infty$
t = time
u = velocity component in the x direction
v = velocity component in the y direction
v_j = liquid velocity at nozzle exit
We_{fd} = Weber number, $\rho_f\, d v_j^2/\sigma$
We_{gd} = Weber number, $\rho_\infty\, d u_\infty^2/\sigma$
x = distance in the airstream direction
y = distance in the direction transverse to the airstream
μ = molecular viscosity
ρ = density
σ = surface tension

Subscripts
b = point of column fracture
f = liquid-phase property
g = gas-phase property
w = property of water
∞ = air property in the freestream

Received Dec. 29, 1995; revision received May 10, 1996; accepted for publication May 18, 1996.

*Research Scientist, 3675 Harmeling Drive. E-mail: peikuanw@possum.appl.wpafb.af.mil. Member AIAA.
†Research Engineer, 3675 Harmeling Drive.
‡Research Scientist, 3675 Harmeling Drive. Member AIAA.
§Senior Research Scientist, Aero Propulsion and Power Directorate.

Introduction

LIQUID jet atomization in an air crossflow has important applications in propulsion systems, including fuel injection in turbojet augmentor sections and ramjet and scramjet combustors.[1–3] In these applications, liquid fuel jets are injected from walls of combustors or bluff body flameholders into the airstream under crossflow conditions. The combustion efficiency of these combustors depends closely on the outcome of the jet breakup process. Additionally, current developments in spray simulation techniques require a basic understanding of breakup mechanisms to construct more realistic spray atomization models. Therefore, the breakup mechanisms of liquid jets in crossflows have to be analyzed and understood. Much work has been done on the characterization of spray appearance,[4–6] penetration heights,[7–12] velocity fields,[13–15] and effects of liquid properties.[16–18] However, the understanding of breakup processes is far from complete, and additional studies of the near-field spray structures are needed to resolve the breakup mechanisms.

Previous studies of liquid injection in crossflows include analyses of liquid jets atomized in both subsonic and supersonic airstreams. Kush and Schetz[4] demonstrated three regimes for liquid jet injection in supersonic crossflows, depending on $\bar{q}$. For smaller $\bar{q}$ (<4), waves determine the jet shape and cannot be treated as simple perturbations. For $\bar{q}$ = 11, waves grow regularly along the surface of the liquid column and spread droplets gradually until the point of fracture. Schetz et al.[5] distinguished waves as leeward and windward and related the windward waves to the liquid acceleration caused by aerodynamic drag forces. Ingebo[6] described the waves as capillary and acceleration waves, and atomization was depicted as a process of forming ligaments from the crests of column waves. These studies established that liquid jets are atomized by the formation of waves caused by aerodynamic forces.

Penetration heights and spray plume trajectories have also attracted considerable attention. Schetz and Padhye[7] performed a momentum analysis on maximum penetration heights and found that the maximum penetration height is the distance required to redirect the liquid jet injection momentum flux to the airstream direction. The penetration height was measured at 6.25 jet diameters downstream and was correlated with $\bar{q}$. In-

gebo[8] found that the maximum penetration is a function of $(Re_{jd}/We_{gd})^{0.7}$. Chelko[9] used a simple dimensional analysis to correlate jet trajectories and found that jet penetration y/d depends on v_j/u_∞, ρ_f/ρ_∞, and x/d. Different correlations were then developed following the same methodology. Hojnacki[1] and Wotel et al.[2] developed a power law for the trajectory correlation, whereas Yates,[3] Baranovsky and Schetz,[10] and Inamura et al.[11] used a logarithmic function. These correlations, however, were all developed based on measurements at axial distances larger than 10 diameters downstream of the nozzle exit, and did not provide information about near-field structure and breakup processes.

Most recently, Chen et al.[12] used a Mie scattering technique to investigate jet trajectories from the nozzle exit to about 60 nozzle diameters downstream, and developed a three-parameter exponential function to account for three spray regimes: 1) the liquid column, 2) ligament, and 3) droplet regimes. Droplet velocities were measured with a particle imaging velocimetry (PIV) technique along the upper boundaries of 1-mm water jets.[13] A technique for the simultaneous velocity measurement of liquid and gas phases was also developed by Chen et al.[14] Inamura et al.[15] measured the velocity of waves on liquid columns by measuring the time interval required for a wave to intersect two pulsating laser beams separated by a preset distance. Their results indicate that liquid waves are dominated by v_j when the column inclination angle from the injection direction is less than 20 deg and by u_∞ when the angle is larger than 40 deg.[15]

Effects of liquid properties were studied by Nejad and Schetz[16,17] for liquid jets in a supersonic crossflow. Surface tension was found to have negligible effects on penetration heights; on the other hand, jet disintegration processes were faster and drop sizes were smaller for liquids with smaller surface tension. Jet penetrations were found to vary within a range of $\pm 15\%$ when μ_f was varied from 1 to 60×10^{-3} kg/m/s. Similar results were also observed by Reichenbach and Horn.[18] Wotel et al.[2] tested jet trajectories of water and JP-7 in subsonic crossflows. JP-7 has a smaller surface tension (31%) and a larger viscosity (216%) than water. Jet trajectories were found to be insensitive to liquid property variations and could be correlated using $\bar{q}$.

The recent development of primary and secondary breakup theories has provided a better understanding of liquid jet breakup processes. The concept of the two-stage jet breakup process has been verified by experimental evidence and the understanding of primary and secondary breakup processes has been improved dramatically.[19–25] When liquid/gas density ratios are large and the liquid jet has very low turbulence intensity, liquid jet breakup processes are caused by wall boundary-layer vorticity along the nozzle passage; when the liquid jet is turbulent the breakup is caused by liquid turbulent eddies.[21] As the gas density increases, the aerodynamic secondary breakup merges with the primary breakup and drop sizes become smaller.[22] Aerodynamic secondary breakup processes have been found to exhibit four major breakup regimes: 1) bag, 2) multimode, 3) shear, and 4) catastrophic breakup.[22–25] Small droplets were stripped along the edge of parent drops and correlations were obtained by approximating the final droplet sizes with the thickness of the boundary layer along the windward side of the droplet surface.[22,23] Since the breakup processes of a liquid jet and a spherical droplet in an airflow are both caused by aerodynamic forces, it is reasonable to apply the general understanding of the aerodynamic secondary breakup to the present problem.

The objective of this study was to investigate the near-field structures of spray plumes to characterize liquid column properties to develop a better understanding of the breakup mechanisms of liquid fuel jets injected into air crossflows. Liquid column waves, trajectories, and breakup locations are the primary interest of the present study because they determine the initial locations of drop dispersion. This paper begins with a description of the apparatus and instrumentation, followed by a discussion of the test conditions. Results of liquid column breakup processes are then discussed, treating liquid column wave behaviors, liquid column trajectories, and column breakup locations. This paper concludes with a summary of the present findings on the breakup processes of liquid jets in subsonic crossflows.

Experimental Methods

Apparatus and Instrumentation

Liquid jets were injected vertically upward into a subsonic wind tunnel with the nozzle exit flush with the tunnel bottom wall. Detailed descriptions of the design and operation of the tunnel, along with measured air velocity fields in the test section, can be found in other studies,[13,26] therefore the following description will be brief. The wind tunnel has a rectangular test section with a cross section of 125×75 mm and a length of 406 mm. Quartz windows were installed on the top and both sides of the test section for laser diagnostics and visualization. Large vacuum pumps were connected to the end of the tunnel to maintain a constant back pressure that could be as low as 20 kPa. The airflow was provided by two large reciprocating compressors that produce a total mass flow rate of up to 2.2 kg/s at 5.1 MPa. The tunnel was operated continuously and the air Mach number was controlled by adjusting a variable-area nozzle device to obtain the correct area ratios at the choked point and the test section.[13] Air pressures and temperatures were measured using strain gauges and k-type thermocouples, which were monitored by a personal computer. The uncertainties of the pressure and temperature measurements were less than 1%, while air axial turbulence intensities were about 3% at the center of the tunnel.[26]

The liquid injection system consisted of a large injection tank, a throttling valve, a rotary flow meter, and a nozzle unit. The injection tank has an internal volume of 0.144 m^3 and is rated for 3 MPa. Before the experiment, test liquids were filled into the injection tank and pressurized with high-pressure air. Liquid volumetric flow rates were controlled by a throttling valve and were measured by a rotary flow meter. The rotary flow meter was calibrated to an uncertainty of less than 2%. Measured liquid volumetric flow rates were used to calculate v_j based on the nozzle exit diameter. The nozzle geometry is sketched in Fig. 1. The nozzle passage has an inlet diameter of 7.5 mm, followed by a 45-deg taper to the specified nozzle exit diameter, followed by a straight section with a length/diameter ratio of 4. The transition from the tapered section to the straight nozzle exit section was rounded to avoid cavitation. These nozzle passages were so designed that the liquid turbulence intensity at the exit is small. Thus, the effects of air crossflows can be studied without the presence of extraneous mechanisms.

Near-field structures and breakup properties were visualized and analyzed using a pulsed shadowgraphic technique with a frequency-doubled Nd:YAG laser as light source. The laser can produce 532-nm laser pulses with a duration of about 10 ns, which is sufficient to freeze the motion of the liquid column and the droplets. Shadowgraphs were obtained in a darkened

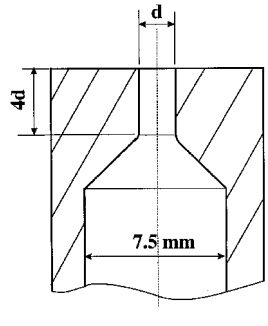

Fig. 1 Nozzle geometry of the present injectors.

Table 1 Summary of test conditions[a]

Liquids	Water	Ethyl alcohol	30% alcohol/water	40% glycerol/water
ρ_f, kg/m^3	996	781	958	1113
$\mu_f \times 10^4$, kg/m/s	8.65	9.57	18.4	36.6
$\sigma \times 10^3$, N/m	63.5	21.7	34.6	65.9
d, mm	0.5, 1.0, 2.0	0.5	0.5, 1.0	0.5, 1.0
v_j, m/s	8.9–37.7	32.0	17.0–38.5	15.7–35.4
u_∞, m/s	70.2–141	69.2, 107	71.5–107	68.1–106
$\bar{q}$	3.38–148	39.9, 98.7	14.0–147	14.5–185
We_{gd}	71–1179	186, 461	140–594	57–287
$We_{fd} \times 10^{-3}$	0.76–11.3	18.4	8.04–20.5	4.16–10.6
$Re_{gd} \times 10^{-3}$	5.72–30.3	13.0	8.87–14.0	4.77–7.56
$Re_{fd} \times 10^{-3}$	3.38–28.4	3.16, 5.08	3.58–10.4	3.00–9.81
$Oh_d \times 10^3$	2.4–4.9	10.4	10.1, 14.3	13.5, 19.1

[a]Air was at 140 ± 4 kPa and 306 ± 3 K in the test section of the wind tunnel, resulting in a density of 1.76 ± 0.05 kg/m^3.

room with an open shutter. A 4 × 5 Speed Graphic camera, loaded with Polaroid type 52 black and white film (ASA 400) was used to record the image. Image magnification was set to be 2.5 by selecting a 250-mm object lens. The field of view (FOV) was limited to 50 × 40 mm to maintain a good spatial resolution of the spray plume. Four shadowgraphs were obtained for each test condition. These images were digitized and analyzed to provide liquid column trajectories and the distances to the column fracture point. The distances to the column fracture point in the downstream and transverse directions were found to vary by 30 and 16% of their mean values, respectively, because of the limited sample sizes and the unsteadiness of the breakup process.

Test Conditions

Test conditions are summarized in Table 1. Liquid jets of water, ethyl alcohol, a 30% alcohol/water solution, and a 40% glycerol/water solution were used to provide a wide range of liquid properties. Mixture concentrations are volume based. Liquid properties were measured for each test liquid before the experiment and are listed in Table 1. Liquid densities were measured using hydrometers that are accurate to 0.5 kg/m^3. Cannon/Fenske viscometers were used to measure liquid viscosities with a measurement uncertainty of less than 0.2%. Liquid surface tensions in air were measured with a ring tensiometer that is accurate to 0.0005 N/m. These liquids provide: liquid densities of 781–1113 kg/m^3, liquid viscosities of $8.65 \times 10^{-4} - 3.66 \times 10^{-3}$ kg/m/s, and surface tensions of 0.0217–0.0659 N/m.

Three nozzles with exit diameters of 0.5, 1.0, and 2.0 mm were manufactured and tested to demonstrate the effects of nozzle diameters. Injection velocities were varied from 8.8 to 38.5 m/s and the air Mach numbers were limited to 0.2, 0.3, and 0.4. The air static pressure was kept to be around 140 kPa. These test conditions yield jet dynamic parameters as follows: $\bar{q}$ of 3.4–185, We_{gd} of 57–1180, We_{fd} of 760–20,500, Re_{gd} of 4.77×10^3–3.03×10^4, Re_{fd} of 3.00×10^3–2.84×10^4, and Oh_d of 2.40×10^{-3}–1.91×10^{-2}. These ranges of test conditions cover most applications of fuel jets in propulsion systems.

Results and Discussion

Results on the near-field jet breakup processes will be discussed in terms of column wave behaviors and column trajectories and breakup locations. Liquid column waves are responsible for droplet formation, whereas the liquid column trajectory and breakup location define the location of these waves. An investigation of these properties is required to understand the jet breakup mechanisms and to construct future spray atomization models.

Column Wave Behaviors

Flow Visualization

Shadowgraphs of liquid jets injected into atmospheric air environments without crossflows were taken to verify the performance of the nozzles used in the present study. A typical shadowgraph of a liquid jet injected at 30 m/s from the 0.5-mm nozzle is shown in Fig. 2; the surface of the liquid column is smooth and no droplet generation or surface protrusion is observed before 26 jet diameters. For nozzles with larger diameters, large-scale waves appear on the column surface, but no droplets are generated. These results demonstrate the near-field structures of these liquid jets without air crossflows and can be used for comparisons with the near-field structures of liquid jets in subsonic crossflows, to be discussed next.

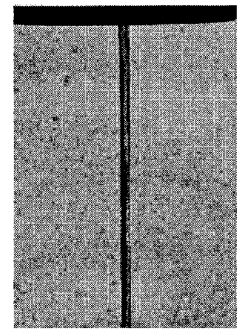

Fig. 2 Injection of a water jet without crossflow (d = 0.5 mm, v_j = 30 m/s).

Figure 3 shows the typical evolution of breakup processes with respect to jet diameters for water jets injected into a crossflow from nozzles with diameters of 0.5, 1.0, and 2.0 mm. $\bar{q}$ is about the same for the three cases (roughly 9.7). For the 0.5-mm jet, the liquid column undergoes column fracture with a mechanism similar to the bag/multimode breakup of a spherical droplet.[22–24] Thin bag-shaped membranes can be identified at several locations, and ligaments are generated from waves with wavelengths larger than the jet diameter. Ligaments break into smaller droplets shortly after the column fracture with a shear-type secondary breakup. Drop sizes then remain relatively constant throughout the FOV. These structures demonstrate with the three previously reported breakup regimes: 1) column, 2) ligament, and 3) droplet regimes.[12]

For the 1.0-mm water jet, the jet penetration and droplet number densities are larger than those of the 0.5-mm jet. Surface waves develop at a short distance above the nozzle exit. These waves initiate from the column periphery and extend to the leeward side; small droplets are stripped away from the end of these waves by the airstream. The liquid column then curves toward the airstream direction and large-scale waves are observed around the liquid column region. The waves on the front side of the column are called windward waves and are caused by aerodynamic acceleration along the column direction.[5] Waves on the leeward side of the column extend for a fairly long distance and generate both ligaments and droplets.

For 2.0-mm water jets, the jet penetration and droplet number density are even larger. The nonuniformity of droplet spatial distributions is clearly seen in the shadowgraph. Ligaments and droplets can be grouped into lumps separated by spatial

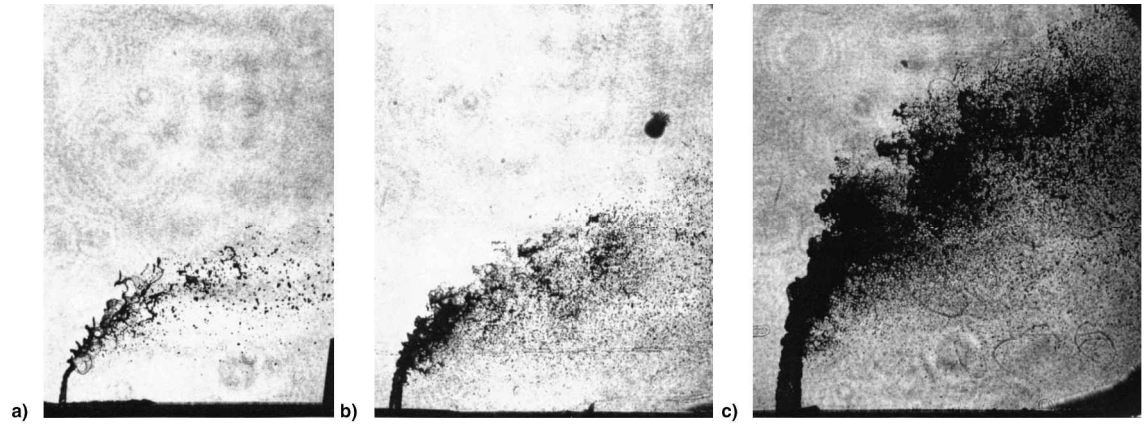

Fig. 3 Injection of water jets from nozzles of various injector diameters: a) d = 0.5 mm, $\bar{q}$ = 9.9, We_{gt} = 71; b) d = 1.0 mm, $\bar{q}$ = 9.4, We_{gt} = 139; and c) d = 2.0 mm, $\bar{q}$ = 10.0, We_{gt} = 281. Water; M_{air} = 0.2; ρ_g = 1.76 kg/m^3.

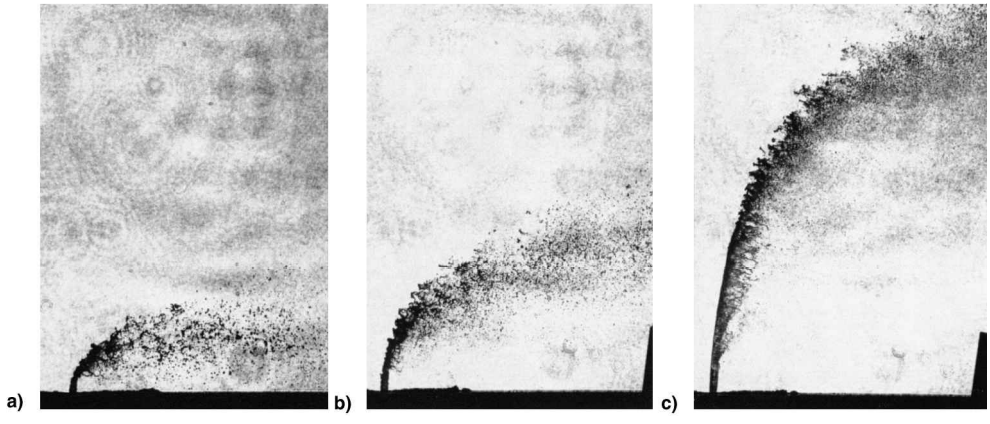

Fig. 4 Injection of water jets at various injection velocities: a) v_j = 9.8 m/s, $\bar{q}$ = 4.8; b) v_j = 19.4 m/s, $\bar{q}$ = 18.5; and c) v_j = 37.9 m/s, $\bar{q}$ = 70.8. Water; d = 0.5 mm; M_{air} = 0.3; ρ_g = 1.76 kg/m^3; We_{gt} = 160.

distances comparable to the wavelengths of column waves. The nonuniformity has been described by Schetz et al.,[5,27] and is a result of the secondary breakup of the clumps of ligaments that are generated by unsteady acceleration waves. It is expected that larger diameter jets require a longer time to become fully developed, whereas droplets are stable and will not undergo secondary breakup.

The breakup process of the liquid column resembles the shear breakup process of a spherical droplet, except that the liquid column is traveling in the transverse direction. For the shear secondary breakup, the drop experiences deformation and then deflection of the periphery in the downstream direction. Smaller droplets are then stripped away from the periphery of these flattened parent drops.[22–25] These phenomena were observed, in the same order, on the liquid column at different transverse locations. The flattening of the liquid column also causes aerodynamic drag forces to increase significantly, because of the increase in the frontal projected area. This may explain why the turning of the liquid column always becomes significant when large scale waves appear on it.

Figure 4 shows shadowgraphs of water jets injected at velocities of 9.8, 19.4, and 37.9 m/s into a Mach 0.3 airstream. The liquid jet penetrates farther into the airstream as v_j increases. At v_j = 9.8 m/s, the liquid column is smooth on both sides of the column immediately after injection. Then, the whole column exhibits large-scale instabilities and is disintegrated by aerodynamic forces. As v_j increases, droplets are generated by waves on the leeward side of the liquid column, even when the windward side exhibits a smooth surface. These waves are generally termed leeward waves,[5] but will be called surface breakup in this study to distinguish them from the breakup process of the liquid column as a whole. This surface breakup process was observed especially when v_j was large (Fig. 4c). Drops from surface breakup are smaller than those generated by column breakup, producing a large drop size variation in the spray plume.

Effects of M_{air} on the breakup processes are demonstrated in Fig. 5 for water jets injected into airstreams with M_{air} of 0.2, 0.3, and 0.4. Liquid injection velocity was 28 m/s for each case. As M_{air} increases, jet penetration decreases, because of the decrease in $\bar{q}$. Both surface and column breakup can be clearly identified on the shadowgraphs. The size of droplets and ligaments and the wavelength of the windward and leeward waves decrease as M_{air} increases as a result of the increase in aerodynamic forces.

Figure 6 summarizes the jet breakup processes of three different liquids: 1) water, 2) the 30% alcohol/water solution, and 3) the 40% glycerol/water solution. Liquid jets were injected at velocities from 35 to 38 m/s, resulting in a range of $\bar{q}$ from 147 to 185. Differences between jet trajectories can be observed in these shadowgraphs. The water jet shows the straightest trajectory, while the glycerol/water solution jet curves more than the others. The column fracture point was located at the highest position for the water jet. For the 30% alcohol/water jet, the onset of surface breakup is closer to the nozzle exit and droplet sizes and ligament nonsphericities are smaller. The 40% glycerol/water jet exhibits longer threads from leeward waves and longer ligaments in the spray plume.

Breakup Regimes

The breakup processes of liquid jets injected into air subsonic crossflows are sketched in Fig. 7. After liquid is injected, the liquid jet may first undergo surface breakup with droplets stripped from liquid surfaces. Acceleration waves then grow

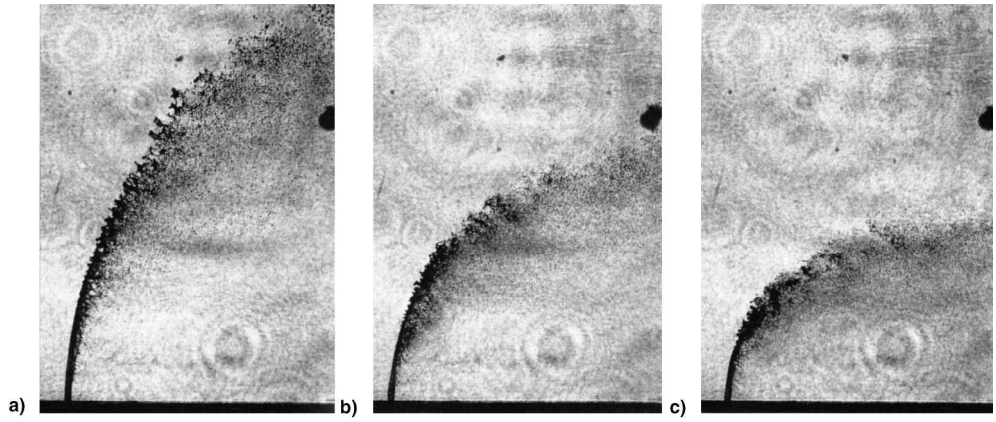

Fig. 5 Injection of water jets into crossflows at various Mach numbers: a) M_{air} = 0.2, $\bar{q}$ = 84, We_{gd} = 75; b) M_{air} = 0.3, $\bar{q}$ = 39, We_{gd} = 160; and c) M_{air} = 0.4, $\bar{q}$ = 22, We_{gd} = 280. Water; d = 0.5 mm; v_j = 28 m/s; ρ_g = 1.76 kg/m^3.

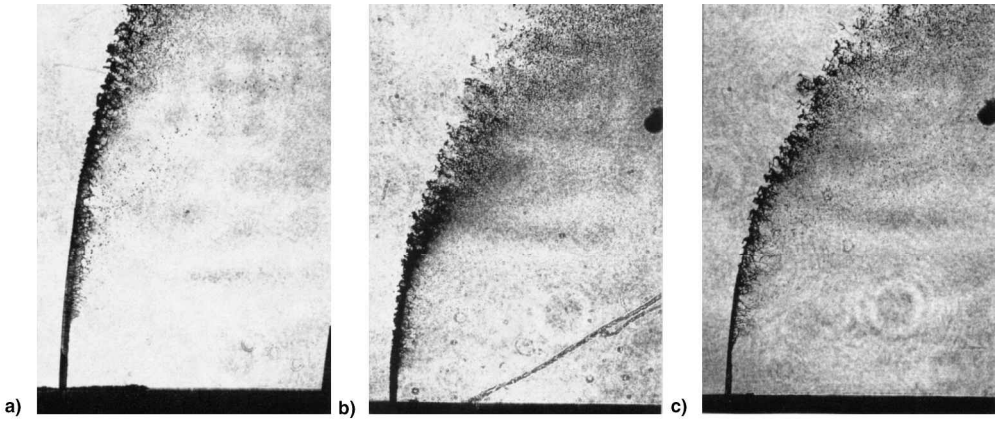

Fig. 6 Injection of various liquids: a) water, $\bar{q}$ = 148, We_{gd} = 75; b) 30% alcohol/water, $\bar{q}$ = 147, We_{gd} = 140; and c) 40% glycerol/water, $\bar{q}$ = 185, We_{gd} = 57. d = 0.5 mm; v_j = 37 m/s; M_{air} = 0.2; ρ_g = 1.76 kg/m^3.

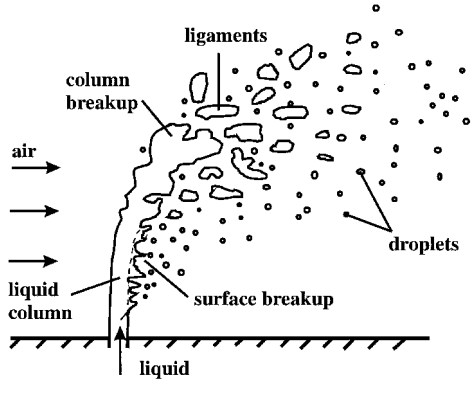

Fig. 7 Sketch of a typical liquid breakup process in an air crossflow.

and the liquid column deforms and is flattened. The liquid column then disintegrates into ligaments and droplets. These near-field structures of the liquid column are summarized and plotted in Fig. 8, according to $\bar{q}$ and We_{gd}. This regime map does not consider breakup mechanisms that are caused by liquid turbulence, cavitation, or effervescence.

When $We_{gd} < 10$, aerodynamic forces are not large as compared to liquid surface tension forces. The liquid jet is curved by aerodynamic forces, which also accelerate the breakup processes caused by capillary forces. This region is referred to as enhanced capillary breakup; examples are given by Kitamura and Takahashi.[28] When We_{gd} is larger than 10, aerodynamic forces dominate the breakup process. The liquid column exhibits breakup behaviors similar to those of the secondary breakup of a spherical droplet.[22–24] Figure 3 demonstrates a bag/multimode column breakup when We_{gd} is small, and shear column breakup when We_{gd} is large. Another interesting feature of the breakup behavior is the surface breakup process. When $\bar{q}$ is small, the liquid jet undergoes column breakup without surface breakup. Surface breakup occurs before the liquid column instabilities when $\bar{q}$ is large (see Figs. 3 and 4). The criterion for the existence of surface breakup is found to be a function of We_{gd}, as shown in Fig. 8, with a slope of -0.81. The onset $\bar{q}$ for surface breakup decreases as We_{gd} increases. However, the straight line plotted in Fig. 8 is provisional and further studies are needed to identify mechanisms for this transition.

Column Trajectories and Breakup Locations

Liquid Column Trajectories

Previous measurements of spray trajectories have emphasized far downstream locations, where small droplets dominate the mixing processes.[1–18] To characterize breakup mechanisms, however, attention must be focused on properties of the liquid column. To understand the liquid column disintegration process, phenomenological analyses were employed to highlight the underlying atomization physics and to provide simple correlations without solving exact and complicated governing equations.

In this study, liquid column trajectories were analyzed by balancing liquid acceleration with aerodynamic drag forces in the airstream direction. Since the liquid column is curved in the downstream direction, the change of liquid velocities is apparently because of aerodynamic drag forces. It is assumed that the liquid column can be modeled as a cylindrical fluid element of the diameter of the nozzle exit d, and of a length

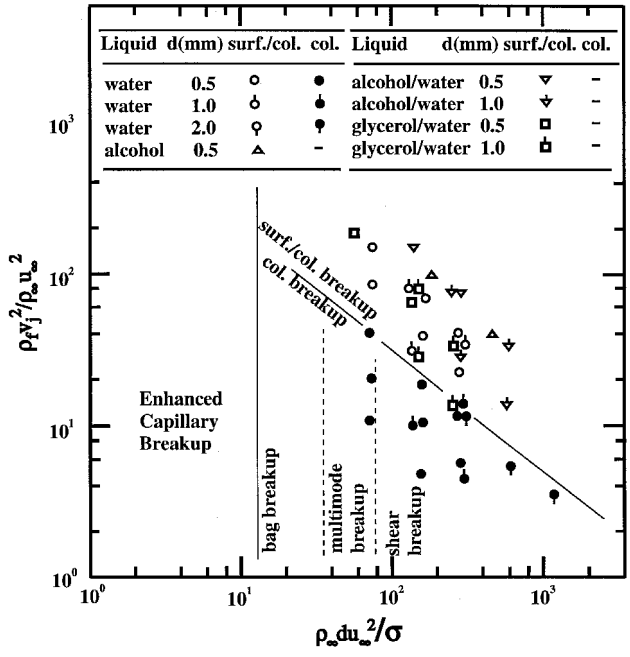

Fig. 8 Regime map of column waves and breakup processes in crossflows.

l. The diameter of the fluid element is also assumed to be a constant. These assumptions neglect mass losses caused by evaporation and droplet removal along the liquid column. For simplicity, the deformation and flattening of the liquid column are accounted for with an averaged drag coefficient, which will be described later. A schematic plot of the force diagram of a liquid element in a crossflow is shown in Fig. 9. The origin of the x and y coordinates is defined at the center of the nozzle exit, with x pointing downstream and y pointing in the transverse direction. The force of gravity is small and negligible when compared with the aerodynamic force. It is further assumed that the transverse velocity of the liquid column remains constant to the column fracture location. By introducing an average C_D, the x-momentum equation can be written as

$$\left(\frac{\rho_f \pi d^2 l}{4}\right)\left(\frac{du_f}{dt}\right) = 0.5 C_D \rho_g (u_g - u_f)[(u_g - u_f)^2 + (v_g - v_f)^2]^{1/2} ld \tag{1}$$

where C_D is an average value of the drag coefficients along the entire length of the liquid column and includes the effects of liquid column deformation, flattening, droplet stripping, and disintegration. For the present test conditions, $(v_g - v_f)^2$ is estimated to be less than 25% of $(u_g - u_f)^2$, and is neglected in the following derivation. Additionally, u_f is estimated to be less than 16% of u_∞ [based on Eqs. (2) and (13), which are discussed later]. Therefore, it is assumed that the variation of $(u_g - u_f)$ is also accounted for in C_D and can be represented by a constant, u_∞. For low Mach number subsonic flows, ρ_g is assumed to have a constant value, ρ_∞. Equation (1) can then be integrated with respect to time to find the velocity component u_f as

$$u_f = (2C_D/\pi)[(\rho_\infty u_\infty^2)/(\rho_f d)]t \tag{2}$$

The axial location of the liquid column can be found by integrating Eq. (2) again as $(u_f = dx/dt)$:

$$x = (C_D/\pi)[(\rho_\infty u_\infty^2)/(\rho_f d)]t^2 \tag{3}$$

As mentioned, the transverse velocity of the liquid column is assumed to be a constant of the value of the injection velocity v_j. Thus, the trajectory can be obtained from Eq. (3) using $y = v_j t$:

$$y/d = \sqrt{(\pi/C_D)(x/d)\bar{q}} \tag{4}$$

The column trajectory follows a parabolic curve as a result of acceleration in the x direction caused by aerodynamic forces.

Liquid column trajectories were measured from the images of shadowgraphs for different liquids and jet operation conditions. The images were digitized and points on the upper surface of the liquid columns were manually located. Twenty points, roughly equidistant in the x direction, were obtained for each image. The points from four images were then combined for trajectory analyses to obtain the best-fit results for each test condition. Equation (4) was rewritten for a linear regression analysis as

$$\frac{y}{(d\bar{q})} = \sqrt{\pi/C_D}\left[\frac{x}{(d\bar{q})}\right]^n \tag{5}$$

Results of the best fits of C_D and n are plotted in Fig. 10 for all the test conditions vs $\bar{q}$. The correlation coefficients of the

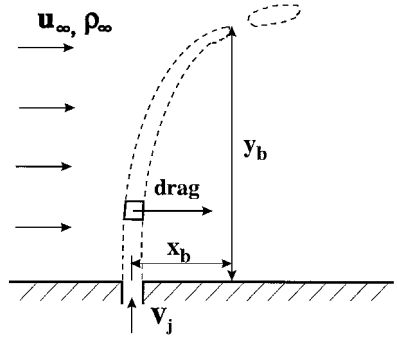

Fig. 9 Sketch of the force diagram for the present phenomenological analysis.

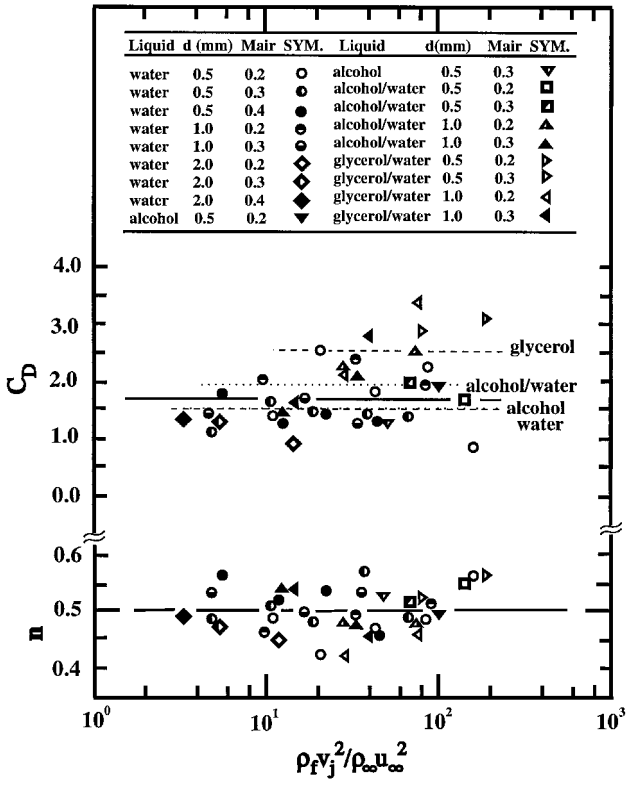

Fig. 10 C_D and n of the fit according to the trajectory analysis.

regression analysis for each test condition were generally larger than 0.97, indicating a valid fitting for the present analysis. The exponents n varied from 0.42 to 0.56 with an average value of 0.50. The standard deviation of the exponents was 0.04 and the 95% confidence interval of the mean value was 0.01. This excellent agreement between the measured and predicted exponent values is encouraging and supports the use of the parabolic function defined previously. For liquids with different viscosities, more scatter was observed in the C_D than in the exponents. Possible reasons are discussed next.

The current measurements also indicate that the effect of surface tension on C_D and column trajectory is not significant, suggesting that the column trajectory variation is dominated by $\bar{q}$ and liquid viscosities. This result agrees with the findings of previous studies.[16–18] An averaged C_D was obtained by averaging the square root of the reciprocal of the C_D; the averaged value was found to be 1.696, resulting in a constant of 1.37 in Eq. (5). This value is of the same order of magnitude as the drag coefficients for flow passing a solid circular cylinder[29] and for the theoretical predictions of liquid injections by Adelberg[30] and Nguyen and Karagozian.[31]

Measured column trajectories are plotted with the correlation of Eq. (5) with the C_D of 1.696 and an exponent of 0.5 in Fig. 11. Measurements were grouped according to liquid type and were obtained from a wide range of test conditions. For water and alcohol, the correlation only underpredicts the results by 5 and 3%, with a scatter of about ±12 and ±10%, respectively. However, the correlation overpredicts by about 8 and 16%, respectively, for the 30% alcohol/water solution and 40% glycerol/water solution. This agrees with the previous discussion of the viscosity dependence of column trajectories as seen in Fig. 6. The results of the 40% glycerol/water solution show a larger scatter (about ±19%) about their mean values. The larger scatter indicates a more unstable nature of the injection process for more viscous liquids.

As shown in Figs. 10 and 11, column trajectories exhibit a systematic variation with respect to μ_f. As μ_f increases, C_D increases and liquid jets penetrate less into the airstream. This phenomenon can be explained considering the thicker liquid boundary layer on the windward side of the jet column of the more viscous liquids. A larger portion of the liquid column is accelerated, therefore, the column curves more sharply into the airstream direction and penetrates less. C_D of the different liquids was summarized and may be represented as

$$C_D/C_{Dw} = 0.984(\mu_f/\mu_{fw})^{0.364} \tag{6}$$

where C_{Dw} and μ_{fw} are 1.51 and 8.65×10^{-4} kg/m/s, respectively. Equation (6) provides a reasonable correlation of the present data; it is of course provisional because it is based on relatively few data. The variations of C_D result in a variation of y of less than 13% because of the square root function in Eq. (4).

Measured trajectories were also tested with existing correlations developed based on results including ligament and droplet regimes. The correlations are summarized as follows: Yates[3] and Baranovsky and Schetz[10] obtained

$$y/d = 1.15\sqrt{\bar{q}}\,\ell n(1 + 6x/d) \tag{7}$$

Geery and Margetts[32] and Hojnacki[1] used

$$y/d = 2.1\sqrt{\bar{q}}(x/d)^{0.27} \tag{8}$$

Chen et al.[12] proposed a three-parameter trajectory function as

$$y/d = 9.91\bar{q}^{0.44}[1 - \exp(-x/d/13.1)] \times [1 + 1.67\exp(-x/d/4.77)][1 + 1.06\exp(-x/d/0.86)] \tag{9}$$

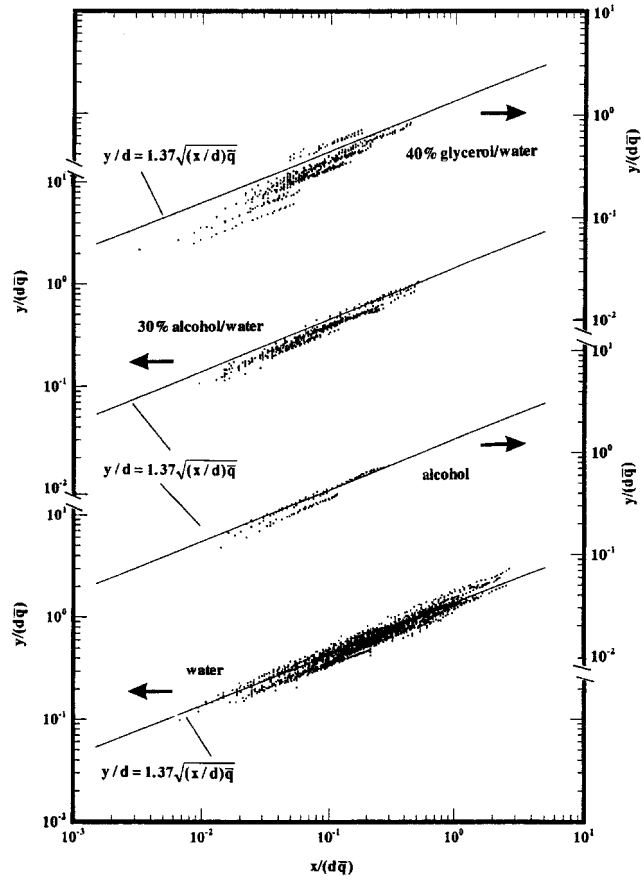

Fig. 11 Comparison of liquid column trajectories of different liquids with the correlation [Eq. (5)].

while Wotel et al.[2] suggested

$$y/d = 1.19\bar{q}^{0.45}(x/d)^{0.45} \tag{10}$$

Equation (10), suggested by Wotel et al.,[2] has a similar functional form as Eq. (5), with a slightly different exponent. However, this correlation is empirical and was developed based on results at locations of about 5–140 jet diameters downstream of the nozzle exit. Ratios of the measured y values to the predicted y values from Eqs. (7–10) were calculated. The averaged values were found to be 0.75, 0.90, 0.75, and 1.45, with standard deviations of 0.14, 0.18, 0.11, and 0.22, respectively. Equation (5) yields a ratio of 1.00 and a deviation of 0.16 based on the same test. Equations (7–10) were developed with emphasis on trajectories at farther downstream locations, where ligaments and droplets dominate the mixing process. The discrepancies between the measured values and the predictions of Eqs. (7–10) were therefore attributed to the differences between drag coefficients and length scales for liquid/air momentum exchanges between the liquid column and the ligament/droplet regimes.

Column Breakup Locations

Column breakup locations will be discussed next in terms of the distances from the nozzle exit to the column fracture point in the x and y directions. To quantify the fracture locations, the shadowgraph images were analyzed. For low-viscosity liquids, the fracture locations were identified without much difficulty by locating the mean location where the liquid column breaks into separate ligaments or droplets. For liquids with smaller surface tensions or larger viscosities, the fracture location becomes more difficult to determine because of larger drop number densities or because of the presence of longer irregularly shaped ligaments. However, the current measure-

ments of x_b and y_b show consistent results within reasonable uncertainties (30 and 16%, respectively).

The column fracture locations were modeled using the time scale for the aerodynamic secondary breakup of a spherical droplet. This approach is plausible since the breakup mechanisms for both columns and droplets are the result of aerodynamic forces. Hsiang and Faeth[23] indicated that the breakup time scale found by Ranger and Nicholls[33] for shear breakup was also applicable for other breakup regimes. The time scale t_b for a droplet with negligible initial streamwise velocity can be written as

$$t_b = 5.0 d_p \sqrt{(\rho_f/\rho_\infty)}/u_\infty \tag{11}$$

where d_p is the drop size before the breakup process.[23]

Time scales for the completion of the secondary breakup are applied to determine the time required for the liquid column to fracture in a crossflow condition. It is assumed that the time required for the column to fracture is a fixed portion of the time required for the completion of the breakup process. Since v_j is assumed to be constant up to the column fracture point, y_b can be obtained by multiplying the breakup t_b with v_j as

$$y_b/d = C_y \sqrt{\bar{q}} \tag{12}$$

where C_y is a proportionality constant. Equation (12) indicates that the normalized distance y_b/d to the fracture point is a function of $\bar{q}$ alone. Present measurements of y_b are plotted in terms of the variables of Eq. (12) in Fig. 12. These results include y_b for several liquids and for a large range of jet conditions, and the prediction agrees reasonably well with the data in view of the relatively large experimental uncertainties. The power of $\bar{q}$ for the correlation of the data is not 0.5 as suggested by Eq. (12), however, and can be represented better by the empirical fit that is shown in Fig. 12:

$$y_b/d = 3.07 \bar{q}^{0.53} \tag{13}$$

The correlation coefficient for the fit is 0.94. The increase in the power of the $\bar{q}$ from 0.50 in Eq. (12) to 0.53 in Eq. (13) is statistically significant, but is not large in view of the approximations used to develop the correlating expression and experimental uncertainties.

A second approach was employed to correlate y_b. The power of $\bar{q}$ was fixed at 0.5 and the values of $y_b/\bar{q}^{0.5}$ were averaged to yield the proportionality constant C_y. C_y was found to be 3.6, 3.02, 3.14, and 4.49 for water, the 30% alcohol/water solution, the 40% glycerol/water solution, and ethyl alcohol, respectively; and standard deviations for these liquids were 0.73, 0.28, 0.27, and 0.32. These values indicate a weak effect of the y distances on liquid properties, although a wider range of liquid properties should be studied to confirm their effects. An overall mean value was obtained to be 3.44, which was used for the theoretical prediction in Fig. 12. The standard deviation of this mean value is 0.71.

The x distance from the nozzle exit to the column fracture point can then be calculated by substituting Eq. (12) into Eq. (5):

$$x_b/d = C_y^2 C_D/\pi = C_x \tag{14}$$

where C_x is a proportionality constant. Present measurements of x_b/d are plotted in terms of $\bar{q}$ in Fig. 13. x_b/d is relatively independent of $\bar{q}$ and agrees with the prediction of Eq. (14). The mean value of x_b/d is 8.06 with a standard deviation of 1.46. Variations in averaged x_b/d of different liquids are around 7%, which is not significant. Measured x_b/d is about 25% larger than the prediction obtained by substituting the values of C_y and C_D into Eq. (14): the discrepancy is primarily because of uncertainties in measurements and correlation processes. A linear regression was made to check the dependence

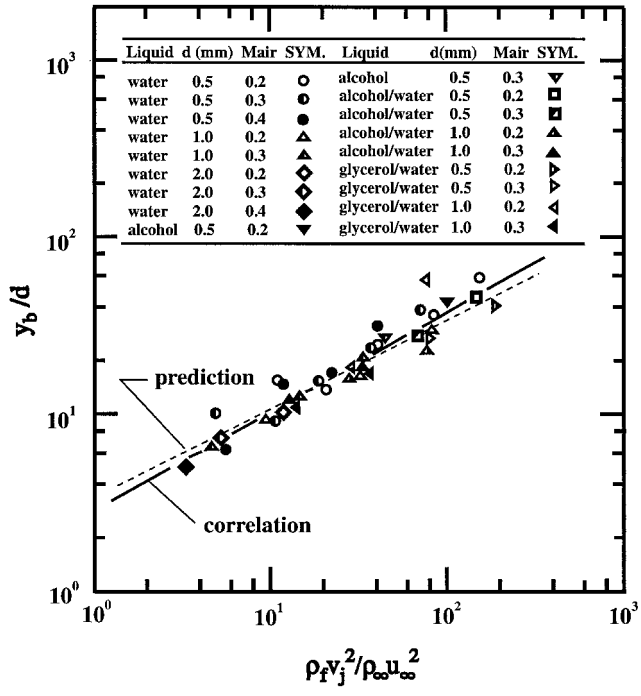

Fig. 12 Column fracture heights y_b/d of liquid jets in air crossflows.

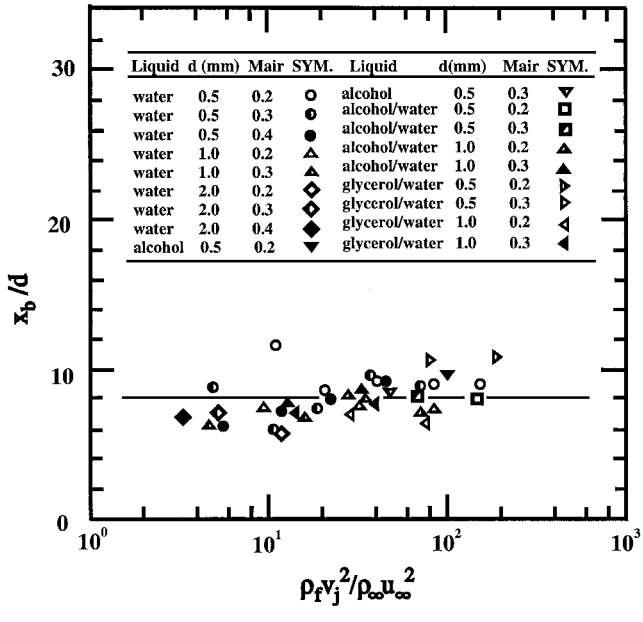

Fig. 13 Column fracture distance x_b/d of liquid jets in air crossflows.

of x_b/d with respect to $\bar{q}$, and the slope of the best fit was 0.07, which is negligible. Therefore, it is concluded that the liquid column always breaks at a distance of 8.06 ± 1.46 jet diameters downstream of the nozzle.

Inamura et al.[11,15] used a contact needle probe to identify the column breakup location and also found that x_b is not sensitive to $\bar{q}$ and liquid jet properties. This phenomenon can be explained by the cancellation of aerodynamic effects on the liquid acceleration and on the column fracture time scale. A larger aerodynamic force increases the liquid acceleration [Eq. (3)], however, it also reduces the time required for the column to fracture [Eq. (11)]. These two effects cancel each other, resulting in a constant x_b. On the other hand, the variation of the liquid injection velocity only affects the liquid jet penetration and does not have significant effects on x_b. The fracture point

marks the boundary between the liquid column and the dispersed-phase regimes. Each regime has its own flow dynamics and a successful spray analysis should consider these differences.

Summary of Correlations

The correlations of the column trajectory and cross fracture locations may be summarized with measured values as follows:

Liquid column trajectory [Eq. (5)]:

$$y/d = 1.37\sqrt{\bar{q}(x/d)}$$

Transverse height of the column fracture point [Eq. (12)]:

$$y_b/d = 3.44\sqrt{\bar{q}}$$

Axial distance to the column fracture point [Eq. (14)]:

$$x_b/d = 8.06$$

Summary and Conclusions

The breakup processes of liquid jets injected into subsonic crossflows were experimentally studied using a pulsed shadowgraphy technique, considering liquid jets of water, ethyl alcohol, a 30% alcohol/water solution, and a 40% glycerol/water solution in subsonic air crossflows. Jet breakup processes, liquid column trajectories before column fracture points, and the distances to column fracture points were investigated. The major conclusions of the study are as follows:

1) The liquid column breakup processes in a crossflow are similar to those of the aerodynamic secondary breakup of a spherical droplet. The liquid column undergoes deformation first and is then flattened and disintegrated by aerodynamic forces. At We_{gd} of about 60, the liquid column breaks into several bag-shaped membranes, similar to the multimode breakup of droplets. At larger We_{gd} conditions, acceleration waves break the column with a shearing process similar to droplet shear breakup.

2) When $\bar{q}$ is large, the liquid jet undergoes surface breakup as droplets are stripped off from the deflected edges of the liquid column before the development of large-scale column waves. For more viscous liquids, these surface waves are more prominent and have very long threads.

3) A momentum analysis was developed to correlate column trajectories by equating the liquid velocity change in the airstream direction caused by aerodynamic drag. The predictions agree with experimental measurements reasonably well within measurement uncertainties. Earlier correlations based on results for far downstream locations were found to be inappropriate for the description of liquid column trajectories before the fracture point.

4) Drag coefficients were inferred by comparing the column trajectory predictions with measured results. Drag coefficients were larger for jets of more viscous liquids. This phenomenon is attributed to the thicker boundary layer on the windward side surface of the liquid column.

5) The column fracture locations were identified by measuring the distances from the nozzle exit to the fracture points. The transverse distances to the fracture point were correlated using the secondary breakup time of a spherical droplet because of the close analogy between the breakup processes of a droplet and those of a liquid column.

6) The x distances to the column fracture point were found to be a constant for the present test conditions. Liquid jets always break at a location of about eight diameters downstream from the nozzle exit, independent of jet injection conditions. The fracture point marks the boundary between the liquid column and the dispersed-phase regimes.

The present results are primarily limited to the liquid jet breakup processes caused by aerodynamic forces. The effects of liquid turbulence and cavitation, and their interactions with aerodynamic effects, were not considered in the present study and should be resolved in the future. Drop sizes after the breakup should also be studied because of their importance for injector designs and spray model validation.

Acknowledgments

This work was sponsored by and performed at the U.S. Air Force Wright Laboratory, Wright–Patterson AFB, Ohio, under Contract F33615-93-C-2300. Assistance from the air facility group of Wright Laboratory is acknowledged. The authors would also like to thank T. H. Chen and M. R. Gruber for helpful discussions, C. D. Carter for lending the Nd:YAG laser for the present shadowgraph study, and W. F. Terry and S. A. McAlpine for helping with tunnel installation. Comments from A. E. S. Creese concerning this paper are also appreciated.

References

[1]Hojnacki, J. T., "Ramjet Engine Fuel Injection Studies," Aero Propulsion Lab., AFAPL-TR-72-76, Wright–Patterson AFB, OH, 1972.

[2]Wotel, G. J., Gallagher, K. E., Caron, S. D., Rosfjord, T. J., Hautman, D. J., and Spadaccini, L. J., "High Speed Turboramjet Combustor Technology Program," Wright Lab., TR-91-2043, Wright–Patterson AFB, OH, 1991.

[3]Yates, C. L., "Liquid Injection into a Supersonic Stream," Aero Propulsion Lab., Vol. 1, AFAPL-TR-71-97, Wright–Patterson AFB, OH, 1972.

[4]Kush, E. A., and Schetz, J. A., "Liquid Jet Injection into a Supersonic Flow," *AIAA Journal*, Vol. 11, No. 9, 1973, pp. 1223, 1224.

[5]Schetz, J. A., Kush, E. A., and Joshi, P. B., "Wave Phenomena in Liquid Jet Breakup in a Supersonic Crossflow," *AIAA Journal*, Vol. 18, No. 7, 1980, pp. 774–778.

[6]Ingebo, R. D., "Aerodynamic Effects of Combustor Inlet-Air Pressure on Fuel Jet Atomization," AIAA Paper 84-1320, June 1984.

[7]Schetz, J. A., and Padhye, A., "Penetration and Breakup of Liquids in Subsonic Airstreams," *AIAA Journal*, Vol. 15, No. 10, 1977, pp. 1385–1390.

[8]Ingebo, R. D., "Penetration of Drops into High-Velocity Airstreams," NASA TM X-1363, 1967.

[9]Chelko, L. J., "Penetration of Liquid Jets into a High-Velocity Air Stream," NACA RM E50F21, 1950.

[10]Baranovsky, S. I., and Schetz, J. A., "An Experimental Investigation of Methods to Increase the Liquid Jet Penetration into Supersonic Flow," Air Force Office of Scientific Research, 78-1300, Bolling AFB, Washington, DC, 1978.

[11]Inamura, T., Nagai, N., Hirai, T., and Asano, H., "Disintegration Phenomena of Metalized Slurry Fuel Jets in High Speed Air Stream," *Proceedings of the 5th International Conference on Liquid Atomization and Spray System*, NIST, Gaithersburg, MD, 1991, pp. 839–846.

[12]Chen, T. H., Smith, C. R., Schommer, D. G., and Nejad, A. S., "Multi-Zone Behavior of Transverse Liquid Jet in High-Speed Flow," AIAA Paper 93-0453, Jan. 1993.

[13]Chen, T. H., Roe, L. A., and Nejad, A. S., "Multifunction Droplet Imaging and Velocimetry System for Spray Jets," *Journal of Propulsion and Power*, Vol. 10, No. 6, 1994, pp. 798–803.

[14]Chen, T. H., Nejad, A. S., Carter, C. D., and Goss, L. P., "A Technique for Simultaneous Velocity Measurement of Liquid and Gas Phases," AIAA Paper 94-0494, Jan. 1994.

[15]Inamura, T., Nagai, N., Watanabe, T., and Yatsuyanagi, N., "Disintegration of Liquid and Slurry Jets Traversing Subsonic Airstreams," *Experimental Heat Transfer, Fluid Mechanics, and Thermodynamics*, edited by M. D. Kelleher et al., Elsevier, New York, 1993, pp. 1522–1529.

[16]Nejad, A. S., and Schetz, J. A., "Effects of Properties and Locations in the Plume on Droplet Diameter for Injection in a Supersonic Stream," *AIAA Journal*, Vol. 21, No. 7, 1983, pp. 956–961.

[17]Nejad, A. S., and Schetz, J. A., "Effects of Viscosity and Surface Tension on a Jet Plume in Supersonic Crossflow," *AIAA Journal*, Vol. 22, No. 4, 1984, pp. 653–659.

[18]Reichenbach, R. E., and Horn, K. P., "Investigation of Injectant Properties on Jet Penetration in a Supersonic Stream," *AIAA Journal*, Vol. 9, No. 3, 1971, pp. 469–472.

[19]Faeth, G. M., "Structure and Atomization Properties of Dense Turbulent Sprays," *23rd Symposium (International) on Combustion*, The Combustion Inst., Pittsburgh, PA, 1990, pp. 1345–1352.

[20]Wu, P.-K., and Faeth, G. M., "Onset and End of Drop Formation Along the Surface of Turbulent Liquid Jets in Still Gases," *Physics*

of Fluids, Vol. 7, No. 11, 1995, pp. 2915–2917.
[21]Wu, P.-K., Miranda, R. F., and Faeth, G. M., "Effects of Initial Flow Conditions on Primary Breakup of Nonturbulent and Turbulent Round Liquid Jets," *Atomization and Sprays*, Vol. 5, No. 2, 1995, pp. 175–196.
[22]Wu, P.-K., Hsiang, L.-P., and Faeth, G. M., "Aerodynamic Effects on Primary and Secondary Breakup," *Liquid Rocket Engine Combustion Instability*, edited by V. Yang and W. Anderson, Vol. 169, Progress in Astronautics and Aeronautics, AIAA, Washington, DC, 1995, pp. 247–279.
[23]Hsiang, L.-P., and Faeth, G. M., "Near-Limit Drop Deformation and Secondary Breakup," *International Journal of Multiphase Flow*, Vol. 18, No. 5, 1992, pp. 635–652.
[24]Krzeczkowski, S. A., "Measurement of Liquid Droplet Disintegration Mechanisms," *International Journal of Multiphase Flow*, Vol. 6, No. 2, 1980, pp. 227–239.
[25]Hinze, J. O., "Fundamentals of the Hydrodynamic Mechanism of Splitting in Dispersion Processes," *AIChE Journal*, Vol. 1, No. 3, 1955, pp. 289–295.
[26]Raffoul, C. N., Nejad, A. S., Gould, R. D., and Spring, A. S., "An Experimental and Numerical Study of the Isothermal Flowfield Behind a Bluff Body Flameholder," American Society of Mechanical Engineers, Paper 95-GT-102, June 1995.
[27]Less, D. M., and Schetz, J. A., "Transient Behavior of Liquid Jets Injected Normal to a High-Velocity Gas Stream," *AIAA Journal*, Vol. 24, No. 12, 1986, pp. 1979–1986.
[28]Kitamura, Y., and Takahashi, T., "Stability of a Liquid Jet in Air Flow Normal to the Jet Axis," *Journal of Chemical Engineering of Japan*, Vol. 9, No. 4, 1976, pp. 282–286.
[29]Kuethe, A. M., and Chow, C.-Y., *Foundations of Aerodynamics, Bases of Aerodynamic Design*, 4th ed., Wiley, New York, 1986, p. 381.
[30]Adelberg, M., "Breakup Rate and Penetration of a Liquid Jet in a Gas Stream," *AIAA Journal*, Vol. 5, No. 8, 1967, pp. 1408–1415.
[31]Nguyen, T. T., and Karagozian, A. R., "Liquid Fuel Jet in Subsonic Crossflow," *Journal of Propulsion and Power*, Vol. 8, No. 1, 1992, pp. 21–29.
[32]Geery, E. L., and Margettes, M. J., "Penetration of a High Velocity Gas Stream by a Water Jet," *Journal of Spacecraft*, Vol. 6, No. 1, 1969, pp. 79–81.
[33]Ranger, A. A., and Nicholls, J. A., "The Aerodynamic Shattering of Liquid Drops," *AIAA Journal*, Vol. 7, No. 2, 1969, pp. 285–290.